

# UC Berkeley

## UC Berkeley Previously Published Works

### Title

Stable electron beam propagation in a plasma column

### Permalink

<https://escholarship.org/uc/item/3wp0f6jv>

### Journal

Physics of Plasmas, 29(4)

### ISSN

1070-664X

### Authors

Diederichs, S  
Benedetti, C  
Esarey, E  
[et al.](#)

### Publication Date

2022-04-01

### DOI

10.1063/5.0087807

### Copyright Information

This work is made available under the terms of a Creative Commons Attribution License, available at <https://creativecommons.org/licenses/by/4.0/>

Peer reviewed

# Stable electron beam propagation in a plasma column

Cite as: Phys. Plasmas **29**, 043101 (2022); <https://doi.org/10.1063/5.0087807>

Submitted: 09 February 2022 • Accepted: 16 March 2022 • Published Online: 04 April 2022

 S. Diederichs,  C. Benedetti, E. Esarey, et al.



View Online



Export Citation



CrossMark

## ARTICLES YOU MAY BE INTERESTED IN

[Perspectives on the generation of electron beams from plasma-based accelerators and their near and long term applications](#)

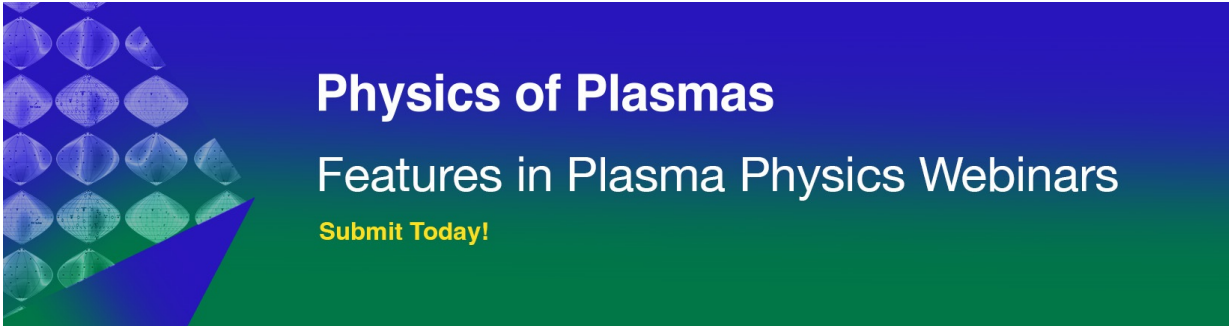
Phys. Plasmas **27**, 070602 (2020); <https://doi.org/10.1063/5.0004039>

[Reduced bandwidth Compton photons from a laser-plasma accelerator using tailored plasma channels](#)

Phys. Plasmas **28**, 123104 (2021); <https://doi.org/10.1063/5.0073622>

[Mathematical tricks for pseudopotentials in the theories of nonlinear waves in plasmas](#)

Phys. Plasmas **29**, 020901 (2022); <https://doi.org/10.1063/5.0078573>



**Physics of Plasmas**  
Features in Plasma Physics Webinars  
**Submit Today!**

# Stable electron beam propagation in a plasma column

Cite as: Phys. Plasmas **29**, 043101 (2022); doi: 10.1063/5.0087807

Submitted: 9 February 2022 · Accepted: 16 March 2022 ·

Published Online: 4 April 2022







View Online



Export Citation



CrossMark

S. Diederichs,<sup>1,2,3,a)</sup>  C. Benedetti,<sup>2</sup>  E. Esarey,<sup>2</sup> M. Thévenet,<sup>1</sup>  J. Osterhoff,<sup>1</sup>  and C. B. Schroeder<sup>2,4</sup> 

## AFFILIATIONS

<sup>1</sup>Deutsches Elektronen-Synchrotron DESY, Notkestr. 85, 22607 Hamburg, Germany

<sup>2</sup>Lawrence Berkeley National Laboratory, Berkeley, California 94720, USA

<sup>3</sup>University of Hamburg, Institute of Experimental Physics, Luruper Chaussee 149, 22607 Hamburg, Germany

<sup>4</sup>Department of Nuclear Engineering, University of California, Berkeley, California 94720, USA

<sup>a)</sup> Author to whom correspondence should be addressed: [severin.diederichs@desy.de](mailto:severin.diederichs@desy.de)

## ABSTRACT

The stability of plasma-based accelerators against transverse misalignments and asymmetries of the drive beam is crucial for their applicability. Without stabilizing mechanisms, even small initial offsets of the drive beam centroid can couple coherently to the plasma wake, grow, and ultimately lead to emittance degradation or beam loss for a trailing witness beam. In this work, we demonstrate the intrinsic stability of a beam propagating in a plasma column. This result is relevant in the context of plasma-based positron acceleration, where a wakefield suitable for the transport and acceleration of a positron witness beam is generated in a plasma column by means of an electron drive beam. The stable propagation of the drive beam is a necessary condition for the experimental implementation of this scheme. The differences and similarities of stabilizing mechanisms in a plasma column compared to a homogeneous plasma are identified via theory and particle-in-cell simulations. Experimental tolerances are given, demonstrating the experimental feasibility of the scheme.

© 2022 Author(s). All article content, except where otherwise noted, is licensed under a Creative Commons Attribution (CC BY) license (<http://creativecommons.org/licenses/by/4.0/>). <https://doi.org/10.1063/5.0087807>

## I. INTRODUCTION

Plasma-based accelerators provide extreme field gradients and enable compact accelerator facilities, potentially drastically reducing their costs. In a plasma-based accelerator, a high-intensity laser pulse<sup>1</sup> or an ultra-relativistic, high-density particle bunch<sup>2</sup> drives a plasma wake, which can be utilized to accelerate a trailing witness bunch. In the so-called blowout regime,<sup>3,4</sup> the driver is strong enough to expel all plasma electrons along the propagation axis, leaving an ion cavity with accelerating and focusing fields on the order of tens to hundreds of GV/m. While high-energy-gain,<sup>5,6</sup> high-efficiency,<sup>7</sup> and low-energy-spread<sup>8</sup> electron acceleration were demonstrated experimentally in this regime, the blowout regime is not applicable to positron acceleration because the ion cavity defocuses positron beams. Application of plasma accelerator technology to an electron-positron collider requires the development of plasma-based methods for positron acceleration. To date, stable, high-quality positron beam acceleration in plasma remains a challenge.

Several positron acceleration concepts have been proposed, including utilizing positron drive beams,<sup>9</sup> hollow-core drive beams<sup>10</sup> or lasers pulses,<sup>11</sup> or the back of the blowout wake.<sup>12</sup> Unfortunately,

none of these concepts support low emittance, low energy spread, and reasonable efficiency simultaneously. Although hollow core plasma channels are a promising candidate,<sup>13,14</sup> they suffer from intrinsic beam-breakup instability due to the absence of focusing fields for the drive beam.<sup>13,15</sup> Using asymmetric drive beams provides stability in at least one direction,<sup>16</sup> but only positron beams with large beam emittances ( $>50 \mu\text{m rad}$ ) have been accelerated in simulations, which is too large for collider applications. The wake generated in a thin, warm, quasi-hollow plasma channel provides accelerating fields for positrons while being robust against instabilities.<sup>17</sup> However, this scheme has been investigated via simulations for a positron beam with several  $\mu\text{m rad}$  emittance and several percent relative energy spread only, i.e., a beam quality insufficient for collider-relevant applications.

Recently, a concept has been proposed that utilizes an electron drive beam and a plasma column to generate positron-accelerating and -focusing wakefield structures that show sub- $\mu\text{m rad}$  emittance and sub-percent energy spread positron acceleration in simulations.<sup>18,19</sup> Since the scheme relies on a cylindrically symmetric wakefield structure, the drive beam stability is of utmost importance. Previous work has reported on the attraction of an electron beam

toward a column of neutral plasma<sup>20</sup> and on the deflection of an electron beam at the plasma-gas boundary.<sup>21–23</sup> Furthermore, a severe misalignment between the column and the electron beam was found to seed the hosing instability.<sup>24</sup>

In this article, we analyze the drive beam stability in depth via theory and particle-in-cell (PIC) simulations. We compare the susceptibility of tilted beams toward the hosing instability in a plasma column and in a homogeneous plasma. We find that the drive beam is self-stabilizing toward tilts and transverse offsets with respect to the center of the plasma column. Finally, we quantify the expected stability of a beam in a plasma column in the context of a potential future experimental realization at FACET-II.<sup>25</sup>

The paper is organized as follows: In Sec. II, we derive an analytical model for the hosing instability in plasma columns and validate it with PIC simulations. Results obtained for the column are compared with that obtained in a homogeneous plasma. In Sec. III, we investigate drive beams with a transverse displacement with respect to the plasma column center. In Sec. IV, we evaluate the stability for a possible experimental implementation. Section V concludes this work.

## II. HOSING FOR A BEAM WITH A TILT IN THE CENTROID

The transverse stability of plasma wakefield accelerators is a long-standing problem that arises due to the coupling between the beam centroid,  $X_b$ , and the plasma wake centroid,  $X_p$ , created by the beam space-charge. For example, an initial displacement of the beam centroid with respect to the wake centroid affects the evolution of the wake centroid itself, which in turn resonantly affects the beam centroid at all phases behind and so forth. The amplification of an initial transverse beam displacement had originally been predicted to grow exponentially in time and along the beam,<sup>26,27</sup> threatening the application of plasma wakefield accelerators. Later, various mechanisms similar to the Balakin–Novokhatsky–Smirnov (BNS) damping in conventional accelerators<sup>28</sup> were identified, predicting saturation of the hosing instability. These include energy spread of the drive beam,<sup>29</sup> non-uniform focusing fields due to ion motion,<sup>30,31</sup> or longitudinally varying focusing fields in the case of large beams sizes.<sup>32</sup>

Modeling the hosing instability has significantly increased the understanding of the relevant physics. In a homogeneous plasma, tilted beams are often used to seed and study the hosing instability. In the following, we further develop and expand the most recent hosing model presented in Ref. 33 to include the effect of a finite-radius plasma column. An accurate description of the plasma response is critical because, as was shown in previous works, the relativistic mass gain/loss<sup>27,33</sup> and the collective behavior of the plasma sheath have been found to mitigate the hosing instability.<sup>33</sup> We use the adapted model to study the stability of a tilted beam against hosing in a column and compare it with the homogeneous case, thereby gaining understanding of the physics relevant in the column case.

We consider a setup where an electron beam propagating in a plasma column drives a wake in the blowout regime, as illustrated in Fig. 1(a), where we plot the plasma charge density  $\rho$  (red-gray color-scale) and the beam density (blue color-scale). Within Secs. II and III, all length scales are normalized to the plasma wave number  $k_p = \omega_p/c$ , all times to the plasma frequency  $\omega_p = \sqrt{4\pi n_0 e^2/m_e}$ , densities to the ambient plasma density  $n_0$ , charges to the elementary charge  $e$ , masses to the electron mass  $m_e$ , fields to the cold,

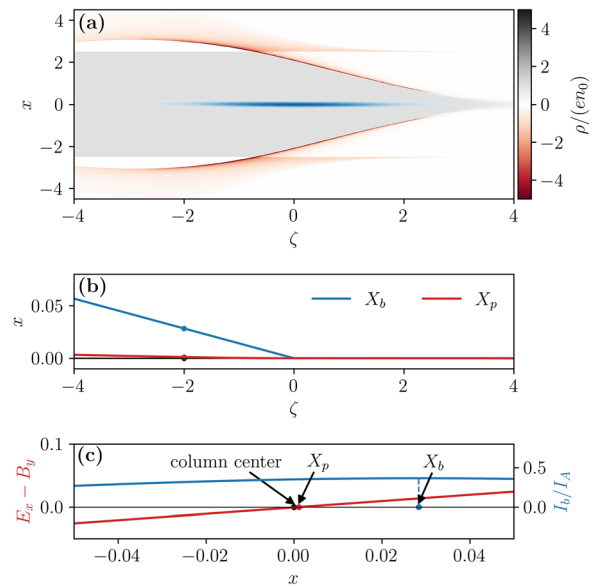


**FIG. 1.** Characterization of the wake structure of a tilted drive beam in a plasma column. (a) Snapshot of the plasma charge density in the  $x$ - $\zeta$ -plane for a drive beam (shown in blue) with an initially tilted beam centroid. (b) The corresponding  $\zeta$ -dependent wake centroid  $X_p$  (red line) and beam centroid  $X_b$  (blue line). Over a longer propagation distance, the small induced offset of  $X_p$  by the beam offset  $X_b$  can build up and lead to strong hosing. (c) Line-out of the beam current profile (blue line) and focusing wakefield (red line) along  $x$  at  $\zeta = -2$ .

non-relativistic wave-breaking field  $E_0 = m_e c \omega_p / e$ , and potentials to  $m_e c^2 / e$ . The beam centroid is tilted transversely, as depicted in Fig. 1(b), which shows the beam centroid  $X_b$  (blue line) and the plasma wake centroid  $X_p$  (red line) along the co-moving variable  $\zeta = z - ct$  ( $z$  is the longitudinal variable,  $c$  is the speed of light in vacuum, and  $t$  is the time). Here, the wake centroid  $X_p(\zeta)$  is defined as the  $x$ -position of the zero-crossing of the focusing field  $E_x - B_y$ . A transverse line-out at  $\zeta = -2$  is presented in Fig. 1(c), where the blue line denotes the beam current profile and the red line a lineout of the transverse wakefield, respectively.

### A. Analytical model

The mathematical model presented in Ref. 33 describes the hosing by means of a set of coupled partial differential equations for the evolution of the  $\zeta$ -dependent plasma wake centroid and the beam centroid, namely,

$$\frac{\partial^2 X_p}{\partial \zeta^2} + C_d(\zeta) \frac{\partial X_p}{\partial \zeta} + \frac{C_p(\zeta)}{2} X_p = \frac{C_b(\zeta)}{2} X_b, \quad (1a)$$

$$\frac{\partial^2 X_b}{\partial t^2} + \lambda(\zeta, t) \frac{\partial X_b}{\partial t} + \Omega_\beta^2(\zeta, t) X_b = \Omega_\beta^2(\zeta, t) X_p. \quad (1b)$$

Both are driven, damped harmonic oscillator-like equations for  $X_p(\zeta, t)$  along  $\zeta = z - ct$  and  $X_b(\zeta, t)$  along  $t$ , respectively.

The coefficients of the beam centroid equation  $\lambda(\zeta, t)$  and  $\Omega_\beta^2(\zeta, t)$  were introduced in Ref. 29. The term  $\lambda(\zeta, t)$  represents the change in the amplitude of the beam centroid oscillation due to relativistic mass gain or loss of the beam electrons, while  $\Omega_\beta^2(\zeta, t)$  accounts

for the effect of the change in the betatron frequency for a changing beam energy.

The coefficients for the plasma wake centroid  $C_{db}$ ,  $C_p$ , and  $C_b$  were introduced in Ref. 33:  $C_p/2$  is the square of the undamped oscillation wavenumber of the system,  $C_b$  describes the coupling of the wake centroid to the beam centroid, and  $C_d$  describes the damping/amplification of the wake centroid oscillation due to the relativistic mass gain/loss of the plasma electrons in the sheath. In the case of a narrow beam in the blowout regime, where the overlap between the beam current density and the electron sheath is negligible, the three wake centroid coefficients are<sup>33</sup>

$$C_p = -\frac{1}{\langle 1 + \Psi \rangle_r} \left[ \left\langle \left( 1 + \frac{J_{z,p}}{\tilde{n} - J_{z,p}} \right) \frac{\partial_r \Psi}{r} \right\rangle_r + \left\langle \frac{\partial_\zeta A_r}{r} \right\rangle_r + \left\langle \frac{\partial_r A_{z,p}}{r} \right\rangle_r \right], \tag{2}$$

$$C_b = \frac{1}{\langle 1 + \Psi \rangle_r} \left\langle \frac{\partial_r A_{z,b}}{r} \right\rangle_r, \tag{3}$$

$$C_d = \frac{\langle \partial_\zeta \Psi \rangle_r}{\langle 1 + \Psi \rangle_r}, \tag{4}$$

with the radial moments being defined as

$$\langle \Phi(r) \rangle_r = \frac{1}{N} \int_0^\infty \tilde{n}(r) \Phi(r) r dr, \tag{5}$$

and where the normalization factor  $N$  is given by

$$N = \int_0^\infty \tilde{n}(r) r dr. \tag{6}$$

Here,  $r$  denotes the radius;  $\Psi$  is the pseudo-wakefield potential;  $A_r$  is the radial component of the vector potential;  $A_{z,b}$  and  $A_{z,p}$  are the longitudinal components of the vector potential associated with the beam and plasma, respectively;  $J_{z,p}$  represents the longitudinal plasma current density; and  $\tilde{n}(r)$  the plasma density profile of the electron sheath. Thus, if the electromagnetic potentials, the plasma current density, and the plasma density profile are known, the coefficients can be calculated. Several analytical models in the blowout regime<sup>34–37</sup> calculate the electromagnetic potentials for a given beam current profile and parameterization of the electron sheath. The model in Ref. 35 assumes an exponentially decaying current and electron density profile in the sheath and has shown good agreement with simulations in the analysis of hosing in a homogeneous plasma.<sup>33</sup> Namely, the electron density in the sheath is assumed to be

$$\tilde{n} = \tilde{n}_s \exp\left(-\frac{r - R_b}{\Delta_\rho}\right) \Theta(r - R_b), \tag{7}$$

where  $R_b$  is the blowout radius,  $\Delta_\rho$  is the sheath thickness,  $\tilde{n}_s$  is the peak sheath electron density, and  $\Theta(x)$  is the Heaviside step function. We adapt the model in Ref. 35 for plasma columns by the following assumptions:

1. For a blowout radius  $R_b$  smaller than the column radius  $R_p$ , the model remains unchanged;
2. For a blowout radius  $R_b$  larger than the column radius  $R_p$ , we assume the ions extend to  $R_p$  and that there is vacuum/non-

ionized gas between  $R_p$  and  $R_b$ . This reduces the peak sheath electron density, since less electrons contribute to it.

The assumptions are illustrated in Fig. 2, which shows the focusing field (blue lines) for the column (solid lines) and a homogeneous plasma (dashed lines) and the respective source for the plasma potential  $S = -(\rho - J_{z,p})$  (black lines), with  $\rho$  being the normalized plasma charge density. The lack of ions in the column between  $R_p$  and  $R_b$  reduces the focusing field at  $R_b$  as well as the peak of the source. The electron sheath is spread over a larger radial extent in case of the column, which is consistently observed in simulations. Using the stated assumptions of the model, the potentials  $A_r$ ,  $A_z$ , and  $\Psi$  for both the plasma column and the homogeneous plasma are derived in the Appendix. Using these potentials and assuming that the thickness of the plasma electron sheath  $\Delta_\rho$  is much smaller than the blowout radius ( $\Delta_\rho/R_b \ll 1$ ) and the thickness of the plasma electron current  $\Delta_J$  spreads over a plasma depth ( $\Delta_J \simeq 1$ , see the Appendix), we obtain the following coefficients in the column for  $R_b < R_p$  (which are equal to that in the homogeneous case<sup>33</sup>):

$$C_p = \frac{1 - R_b'^2}{4} - \frac{\Delta_\rho}{4R_b} \left[ 1 + \Lambda - \frac{R_b'^2}{4} (1 - R_b'^2 - 2R_b R_b' + R_b'^2) \right] + \mathcal{O}\left(\frac{\Delta_\rho^2}{R_b^2}\right), \tag{8}$$

$$C_b = \frac{\Lambda}{R_b^2} \left[ 1 - \Delta_\rho \left( \frac{2}{R_b} + \frac{R_b}{4} \right) \right] + \mathcal{O}\left(\frac{\Delta_\rho^2}{R_b^2}\right), \tag{9}$$

$$C_d = \frac{R_b'}{4} \left[ R_b - \frac{\Delta_\rho}{2} \left( \frac{R_b^2}{2} - 1 \right) \right] + \mathcal{O}\left(\frac{\Delta_\rho^2}{R_b^2}\right), \tag{10}$$

with  $R_b'(\zeta) = \partial_\zeta R_b(\zeta)$ ,  $\Lambda(\zeta) = 4I_b/I_A$  the integrated beam current, and where  $I_A = m_e c^3/e \simeq 17$  kA is the Alfvén current. Note that the coefficient  $C_p$  was rewritten in comparison with Eq. (36) in Ref. 33 to highlight the differences of the coefficient in the plasma column.

In the plasma column with  $R_b > R_p$ , we obtain the new coefficients

$$C_p = \kappa \frac{1 - R_b'^2}{4} - \frac{\kappa \Delta_\rho}{4R_b} \times \left[ 1 + \Lambda - 4R_b'^2 - \frac{R_p^2}{4} (1 - R_b'^2 - 2R_b R_b' + R_b'^2) \right] + \mathcal{O}\left(\frac{\Delta_\rho^2}{R_b^2}\right), \tag{11}$$

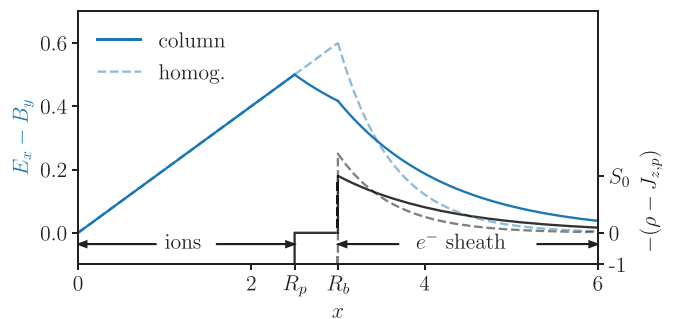


**FIG. 2.** Source term  $S = -(\rho - J_{z,p})$  (black lines) as assumed in the model and resulting focusing field (blue lines) in a plasma column (solid lines) and a homogeneous plasma (dashed lines). In a plasma column with a radius  $R_p$  smaller than the blowout radius  $R_b$ , the focusing field is reduced at the blowout radius.

$$C_b = \frac{\Lambda}{R_b^2} \left[ 1 - \Delta_\rho \left( \frac{2}{R_b} + \frac{\kappa R_b}{4} \right) \right] + \mathcal{O} \left( \frac{\Delta_\rho^2}{R_b^2} \right), \quad (12)$$

$$C_d = \frac{\kappa R_b'}{4} \left[ R_b - \frac{\Delta_\rho}{2} \left( \frac{R_p^2}{2} + 3 \right) \right] + \mathcal{O} \left( \frac{\Delta_\rho^2}{R_b^2} \right), \quad (13)$$

with  $\kappa = R_p^2/R_b^2 < 1$ . A qualitative comparison of the stability in the column versus the homogeneous plasma based on the coefficients alone is difficult, because the plasma column consistently features a larger sheath thickness  $\Delta_\rho$  than the homogeneous plasma, which can be attributed to the larger spread in the electron trajectories in the sheath due to the reduced focusing field.<sup>18</sup>

### B. Comparison with simulation results

For a comparison of the transverse beam stability in a plasma column and in a homogeneous plasma, we employ three-dimensional particle-in-cell (PIC) simulations performed using the quasi-static PIC code HiPACE++.<sup>38</sup>

We consider beam parameters that have been used to demonstrate high-quality positron acceleration<sup>18,19</sup> and introduce a tilt in the bunch distribution to seed the hosing instability. The beam has a bi-Gaussian distribution with  $\sigma_{x,y} = 0.1$ ,  $\sigma_z = 1.41$ ,  $I_b/I_A = 1$ , it has a mean energy of  $\gamma_0 = 20\,000$ , and the emittance is such that the beam is matched in the focusing field of a blowout wake. The initial centroid of the beam is linearly tilted for  $\zeta < 0$  according to  $X_{b,0} = 0.014 \times \zeta \Theta(-\zeta)$ . The beam is sampled with  $10^7$  macro-particles. The computational domain is  $(-16, 16) \times (-16, 16) \times (-6, 6)$  in  $x \times y \times \zeta$  in case of the plasma column and  $(-8, 8) \times (-8, 8) \times (-6, 6)$  in case of a homogeneous plasma. In both cases, the mesh resolution is  $0.0078 \times 0.0078 \times 0.0012$ . The plasma column has a radius of  $R_p = 2.5$  and is modeled by 25 macro-particles per cell. The homogeneous plasma is modeled by 4 macro-particles per cell. The numerical parameters were chosen to ensure convergence, which is reached for different parameters in the column and the homogeneous plasma. The ion background is assumed immobile. The beam is advanced in both cases by a constant time step of  $\Delta t = 10$ .

First, the effect of the beam tilt on the wake centroid is compared in the column case and in the homogeneous plasma case by integrating Eq. (1a) backwards in  $\zeta$  from the start of the tilt to the tail of the beam. To calculate the coefficients  $C_p$ ,  $C_d$ , and  $C_b$  in Eq. (1a),  $R_b(\zeta)$  is extracted from the first time step of a PIC simulation using a beam without a tilt. The slope of the blowout radius  $R_b'(\zeta)$  is calculated from the extracted  $R_b(\zeta)$ . The parameterization of the electron sheath using Eq. (7) is in reasonable agreement with the simulation for  $\Delta_{\rho,h} = 0.25$  and  $\Delta_{\rho,c} = 0.5$  for the homogeneous plasma and plasma column, respectively. We compare the predicted wake centroid from the model (solid lines) with wake centroid from the simulations (dashed and dashed-dotted lines) in Fig. 3. The wake centroid is extracted by the interpolation to the zero crossing of the transverse wakefield  $E_x - B_y$ . The model shows reasonable agreement with the simulations. Both the model and the PIC simulation show that the wake centroid displacement in the column is smaller than in the homogeneous plasma. This indicates that a beam propagating in a column is less prone to the hosing instability than in a homogeneous plasma due to the larger sheath thickness in the column case.

To confirm these findings, we solve the coupled equations Eqs. (1a) and (1b). During the numerical integration of Eq. (1b) in  $t$ , at

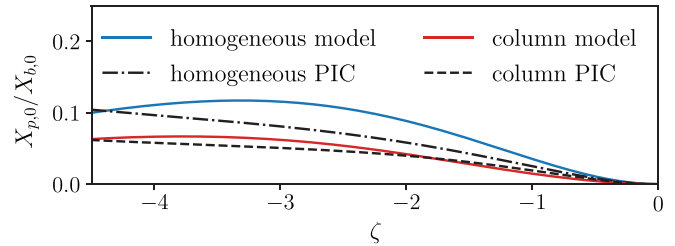


**FIG. 3.** Wake centroid as a function of  $\zeta$  for the beam shown in Fig. 2. In the model, the sheath thicknesses are assumed to be  $\Delta_{\rho,h} = 0.25$  and  $\Delta_{\rho,c} = 0.5$  for the homogeneous case and the column case, respectively. The wake centroid deviation due to the beam tilt is smaller for the plasma column than in a homogeneous plasma, indicating a higher stability in the column. This feature is observed in simulations and is well captured by the model.

each time step, we integrate Eq. (1a) in  $\zeta$  to calculate the wake centroid offset. To calculate  $\lambda(\zeta, t)$  (cf. Ref. 29) in Eq. (1b), we additionally extract the accelerating field  $E_z$  from the PIC simulation with the aligned beam. We evaluate the beam centroid at the position of the tail  $X_{b,tail}$ , which is most susceptible to the hosing instability, and compare it with the PIC simulation results. We define the tail in the simulation as  $X_{b,tail} \equiv X_b(-4.26 < \zeta < -4.20)$ , while we can directly evaluate it in the model at  $\zeta = -4.23$ .

The model (black lines) shows good agreement with the simulations (blue lines for homogeneous plasma and red lines for plasma column), as shown in Fig. 4. As it can be seen in Figs. 4(a) and 4(b), the envelope of the oscillation in the homogeneous plasma has a higher slope than in the column and reaches its maximum after  $\approx 40 \omega_{\beta,0}^{-1}$ , while it takes  $\approx 50 \omega_{\beta,0}^{-1}$  in the column. Here,  $\omega_{\beta,0}$  denotes the initial (i.e., at injection) betatron frequency of the beam. Both cases saturate at roughly two times the initial offset. The presence of an initial uncorrelated relative energy spread detunes the oscillation,<sup>29</sup> suppressing the hosing. For instance, an initial energy spread of  $\sigma_\gamma/\gamma_0 = 3\%$  damps the oscillation in both the homogeneous plasma and the column case, as shown in Figs. 4(c) and 4(d). Here, the oscillation envelope is damped quicker in the column, which we attribute to the reduced coupling (see Fig. 3). Besides reducing the hosing at the tail, an uncorrelated energy spread also prevents the emergence of a wave-like pattern in the beam profile, which can be seen in the video of the full evolution of the bunches in the [supplementary material](#).

In summary, we find that beam propagation in the column case is more robust against hosing seeded by a tilt in the beam centroid compared to the homogeneous plasma case. Our model demonstrates that this is mostly due to the increased sheath thickness in the plasma column, leading to a decreased coupling of the wakefield centroid  $X_p$  to the beam centroid  $X_b$ . However, the column has an additional constraint in comparison with the homogeneous plasma, namely, that the propagation axis of the beam must be aligned with the center of the column. The stability for a transverse displacement of the beam with respect to the column axis is discussed in Sec. III.

### III. HOSING FOR A BEAM NOT ALIGNED WITH THE COLUMN AXIS

The transverse displacement of the electron beam with respect to the plasma column axis is a problem that may arise in experiments due to machine jitters. A transversely misaligned beam that drives a

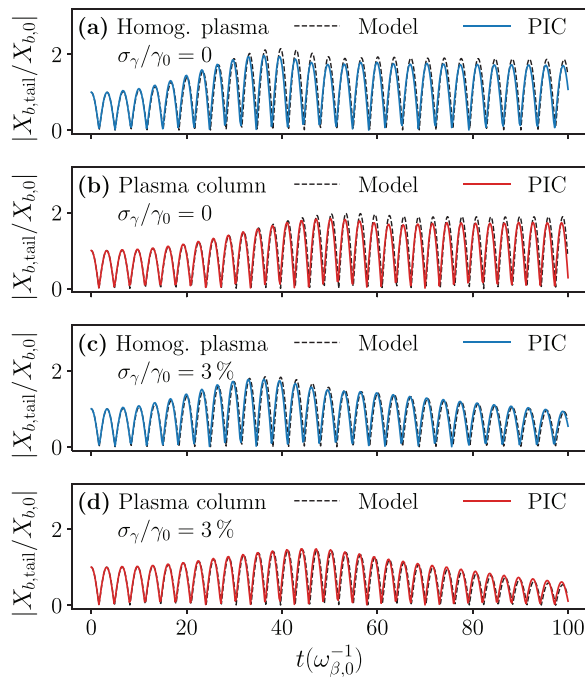


**FIG. 4.** Comparison between the evolution of  $X_{b,tail}$  in the model and the simulation in (a) a homogeneous plasma and (b) the column without an initial energy spread. The oscillation in the plasma column rises less steeply than in the homogeneous plasma but saturates at the same value of roughly two times the initial offset. (c) and (d) Show the results for an initial uncorrelated energy spread of  $\sigma_\gamma/\gamma_0 = 3\%$ . The detuning of the oscillation due to the uncorrelated, relative energy spread has a greater effect in the plasma column and leads to oscillations with an amplitude slightly smaller than that in the homogeneous plasma.

wake in the blowout regime experiences a restoring force toward the column center. In fact, when all plasma electrons of the column are expelled, the majority of the background ions are located on the opposing side of the column with respect to the location of the displaced beam. As the transverse wakefields are mostly caused by the ion distribution, the wake centroid  $X_p$  is not aligned with the beam centroid  $X_b$  but shifted toward the column center. As a consequence,  $X_p$  depends on the co-moving variable  $\zeta$ , since the ion distribution depends on the blowout radius, as illustrated in Fig. 5. Therefore, the head and the tail of the beam are experiencing different restoring forces, which potentially seed the hosing instability.

The analytical model derived in Sec. II is not applicable in this case. In the solution of the coupled centroid equations, the integration has to begin at the start of the beam displacement, which is at the head of the beam. However, in this location, the assumption that the electron sheath is much smaller than the blowout radius ( $\Delta_\rho \ll R_b$ ) is not fulfilled anymore, rendering the model inaccurate. Therefore, PIC simulations were used to investigate the stability of a transversely displaced beam.

The parameters of the beam considered for this study are the ones introduced in Sec. II B, except for the uncorrelated energy spread that has been set to zero, and a beam size of  $\sigma_x = 0.05$ . The initial transverse beam offset with respect to the column is set equal to one root-mean-square (rms) size of the beams, namely,  $X_{b,0} = \sigma_x = 0.05$ .

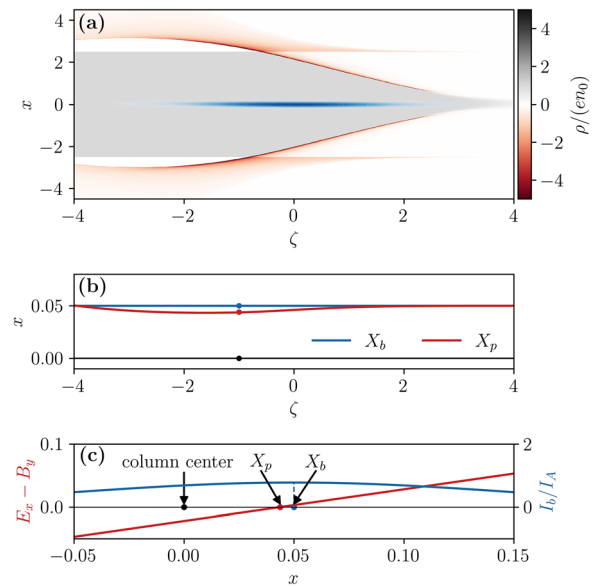


**FIG. 5.** Characterization of the wake structure of a beam with a transverse offset with respect to the column axis. (a) Snapshot of the plasma charge density in the  $x$ - $\zeta$ -plane for a beam (shown in blue) with an initial transverse offset of  $X_b = 0.05$  with respect to the plasma column center. (b) The resulting  $\zeta$ -dependent wake centroid  $X_p$  (red line) that lays between the beam centroid  $X_b$  (blue line) and the center of the column (black line), leading to an attraction of the beam toward the center of the column. (c) Lineout of the beam current profile (blue line) and focusing wakefield (red line) along  $x$  at  $\zeta = -1$ .

The beam is advanced in the plasma column for 2000 time steps with an adaptive time step, resolving each energy-dependent betatron period of the beam with 81 temporal steps. The evolution of the bunch centroid at the tail of the beam,  $X_{b,tail}$ , is shown in Fig. 6(a). As indicated in Fig. 5, the tail of the beam drifts toward the column axis and hosing is seeded. Using an immobile ion background (dashed line), the induced hosing grows initially and saturates at an amplitude on the order of the initial offset. When ion motion is enabled (assuming a Helium plasma, solid line), the oscillation is damped, leaving dominantly a drift toward the column axis. The final  $\zeta$ -dependent bunch centroid is shown in the inset of Fig. 6(a). As predicted by the wake centroid  $X_p$  in Fig. 5, the tail of the beam has drifted closer to the column axis than the head. The  $\zeta$ -dependent temporal evolution of the full bunch is shown in Fig. 6(b). We see that while the tail and the center of the bunch undergo oscillations, the head slowly drifts toward the axis. The oscillations are damped, leaving only a slow drift toward the column axis.

The damping of the oscillation is caused by the detuning effect associated with the motion of background Helium ions.<sup>39–41</sup> The originally uniform background ion distribution is perturbed by the strong space charge fields of the bunch, leading to  $\zeta$ -dependent, non-linear focusing fields. Any longitudinal dependence of the focusing fields causes decoherence of the centroid oscillations,<sup>31,32,42</sup> which is similar to the BNS damping mechanism<sup>28</sup> in conventional accelerators. While the longitudinal variation of the focusing fields for small, high-density drive beams is caused by ion motion, larger, less-intense drive beams can be subject to longitudinally varying focusing fields due to the fact

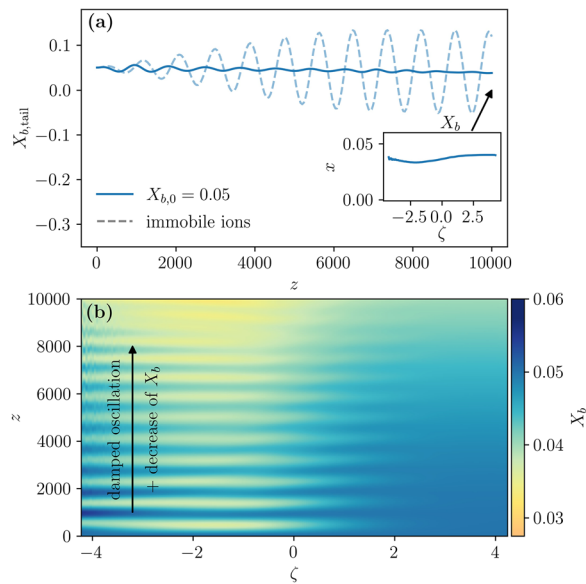


**FIG. 6.** Evolution (a) of the beam centroid at the tail of the beam  $X_{b,tail}$  along the propagation distance for an initial offset of  $X_{b,0} = \sigma_x = 0.05$  assuming an immobile ion background (dashed line) and with mobile ions in a Helium plasma (solid line). The inset shows the final slice-dependent beam centroid. Waterfall plot (b) with the evolution of the beam centroid for  $X_{b,0} = 0.05$  in Helium vs longitudinal coordinate (horizontal axis) and propagation distance (vertical axis). The beam centroid decreases via a damped oscillation toward the column center.

that their head is not experiencing a full blowout wake, and this can suppress the hosing instability, as discussed in Ref. 32.

In summary, an initially transversely displaced electron beam in a plasma column is attracted by the column center, but seeds the hosing instability by inducing a longitudinal dependence in the wake centroid  $X_p$ . However, multiple damping mechanisms cause decoherence of the oscillation, such as ion motion, energy spread, or the head not being in the blowout wake. These processes mitigate the hosing instability and lead to an overall stable propagation of the beam in the plasma column.

#### IV. ASSESSMENT OF STABILITY FOR FACET-II BEAM PARAMETERS

The demonstrated stability against tilts and transverse offsets makes plasma columns a promising candidate for positron acceleration. Currently, FACET-II<sup>25</sup> is the only beam-driven plasma wakefield accelerator facility that plans to accelerate positrons. Using electron drive beams similar to those available at FACET-II, we test both transverse offsets as well as pointing jitters to evaluate tolerances in a possible experiment. Using SI units in this section, the beam is assumed to be bi-Gaussian with  $\sigma_{x,y} = 10 \mu\text{m}$ ,  $\sigma_z = 20 \mu\text{m}$ , has a charge of  $Q_b = 3 \text{ nC}$ , a mean energy of  $\gamma_0 = 20\,000$ , an initial emittance of  $\epsilon_0 = 10 \mu\text{m rad}$ , and an uncorrelated relative energy spread of  $\sigma_\gamma/\gamma_0 = 3\%$ . We consider a Helium plasma column with a density of  $1 \times 10^{17} \text{ cm}^{-3}$  and with a radius of  $R_p = 2.5 k_p^{-1} = 42 \mu\text{m}$ . Helium is used owing to its high ionization threshold: for the given beam parameters, other gases would be ionized outside of the column by the driven wakefield (which exceeds the radius of the column) causing the

column to expand and deteriorate the positron accelerating and focusing fields.

Three different offsets are tested in PIC simulations with the same numerical parameters as in Sec. II B. The evolution of the full beam centroid (a) and the centroid measured at the tail (b) are shown in Fig. 7. Here, the tail is defined as  $X_{b,tail} = X_b(-62 \mu\text{m} < \zeta < -58 \mu\text{m})$ . The blue line corresponds to a small initial offset,  $X_{b,0} = 1 \mu\text{m}$ , the red line to an offset equal to a rms size of the beam,  $X_{b,0} = \sigma_x = 10 \mu\text{m}$ , and the green line to an offset equal to half the column radius,  $X_{b,0} = 0.5 R_p = 21 \mu\text{m}$ . Simulations show that in all cases, an oscillation is induced, which, as expected, is more pronounced at the tail of the beam. However, even for an initial misalignment of  $0.5 R_p$  (green line), which significantly perturbs the wakefield, the drive beam does not breakup, and the seeded hosing is mitigated. We find that, in this case, the mitigation is not caused by ion motion, but rather by the uncorrelated energy spread developing as the beam propagates in the plasma. Although the beam is slightly pulled toward the axis, the drift is not sufficient to compensate and cancel the initial offset. For the presented cases, the beam energy is partially depleted at the end of the propagation distance.

Notably, the induced oscillation scales with the initial offset. Although offsets by a large fraction of the column radius significantly distort the wakefield behind the bunch, the intrinsic stability of the bunch is an important finding. In combination with the scaling of the oscillation with the initial offset, the intrinsic stability allows for the alignment of the beam via active feedback loops.<sup>24</sup> The emitted betatron radiation by the oscillating bunch scales with the oscillation amplitude, and, thus, with the initial offset, allowing for alignment of the electron beam and the plasma column by minimizing the emitted betatron radiation.

We also tested the stability of the beam against pointing jitters, modeled by adding an initial normalized transverse momentum  $u_x$  to the beam particles. It is expected that the maximum pointing angle  $X'_b = u_x/u_z$  to achieve stable beam propagation should be much smaller than the ratio of the column radius  $R_p$  and the plasma length  $L_p$ , i.e.,  $X'_b \ll R_p/L_p$ . Here,  $u_z$  is the mean normalized longitudinal

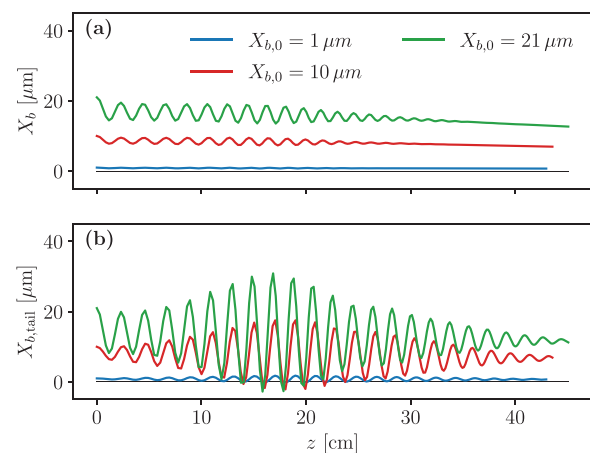


**FIG. 7.** Evolution of the (a) full beam centroid and (b) beam centroid measured at the tail of the beam for different offsets. Despite offsets of large fractions of the column radius, the overall propagation in a plasma column is stable.



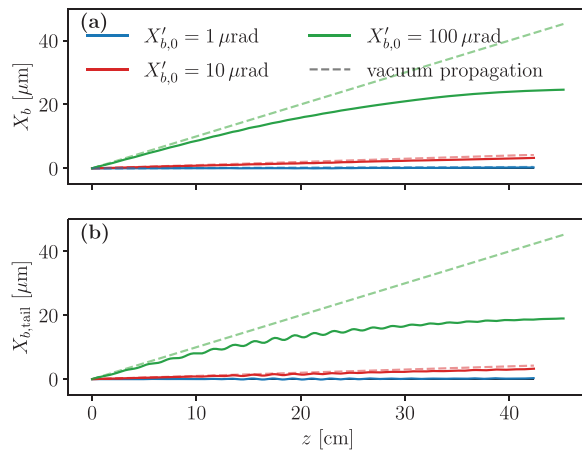


**FIG. 8.** Evolution of the (a) full beam centroid and (b) beam centroid measured at the tail of the beam for different offsets. The column affects the beam propagation only for large pointing jitters.

momentum of the beam. A plasma length of  $L_p = 42$  cm is assumed, such that  $R_p/L_p = 10^{-4}$ . Three different pointing angles are used to study the pointing jitter. The evolution of the full beam centroids (a) and the centroids measured at the tail (b) are shown in Fig. 8. The blue line corresponds to an initial pointing angle of  $X'_{b,0} = 0.01 R_p/L_p = 1 \mu\text{rad}$ , the red line to an initial pointing angle of  $X'_{b,0} = 0.1 R_p/L_p = 10 \mu\text{rad}$ , and the green line to an initial pointing angle of  $X'_{b,0} = R_p/L_p = 100 \mu\text{rad}$ . The dashed lines indicate the vacuum propagation, which was calculated analytically assuming ballistic propagation in vacuum.

For the small and medium pointing angles, the propagation of the centroids hardly differs from that in vacuum. For the large pointing angle of  $X'_{b,0} = R_p/L_p$ , the beam centroid significantly deviates from the column axis. In contrast to the vacuum propagation, propagation in the plasma column results in the centroid trajectory being bent toward the column center. This affects only the center and tail of the beam, while the head still propagates almost unchanged away from the column axis, as shown in the videos in the [supplementary material](#) and in agreement with previous studies.<sup>21–23</sup> Therefore, the initial assumption to achieve stable beam propagation that the pointing jitter should be much smaller than  $R_p/L_p$  was verified. In the context of the presented parameters, a pointing jitter of  $\leq 10 \mu\text{rad}$  is required to allow for stable wakefield structures usable for positron acceleration.

In summary, beam parameters similar to those available at FACET-II predict stable beam propagation for even large offsets and moderate pointing jitters. Large offsets or significant pointing jitters deteriorate the wakefield structure and, therefore, a positional alignment on the  $\mu\text{m}$ -level and an angular alignment on the  $\leq 10 \mu\text{rad}$ -level are required for positron-relevant applications. The implications of a misaligned drive beam on the quality of a potential trailing positron beam will be addressed in detail in a forthcoming work.<sup>43</sup>

## V. CONCLUSION

In this work, we have extended an existing model to describe the hosing instability to plasma columns and have validated the model by

means of PIC simulations. We found that plasma columns are in fact more stable against hosing of tilted beams than homogeneous plasmas because of the increased sheath thickness in the column. However, the propagation axis of the beam needs to be aligned with the central axis of the column. A transversely misaligned drive beam is attracted toward the column center with longitudinally varying forces. Although hosing is seeded, it is efficiently damped by various BNS-like mechanisms, including ion motion<sup>31</sup> or energy spread of the beam.<sup>29</sup> Finally, we have evaluated the tolerance for misalignment of an electron beam for the experimental realization at FACET-II. We found that even for large offsets, the beam is stable. The scaling of the oscillation with the initial offset allows for alignment via active feedback loops. The demonstrated overall stability of an electron beam in a plasma column is an important step toward the experimental realization of positron acceleration in a plasma column.

## SUPPLEMENTARY MATERIAL

See the [supplementary material](#) for videos of the full evolution of the tilted bunches from Sec. II.

## ACKNOWLEDGMENTS

We gratefully acknowledge helpful discussions with T.J. Mehrling, A. Martinez de la Ossa, and S. Gessner. This work was supported by the Director, Office of Science, Office of High Energy Physics, of the U.S. Department of Energy, under Contract No. DE-AC02-05CH11231 and used the computational facilities at the National Energy Research Scientific Computing Center (NERSC). We gratefully acknowledge the Gauss Centre for Supercomputing e.V. ([www.gauss-centre.eu](http://www.gauss-centre.eu)) for funding this project by providing computing time through the John von Neumann Institute for Computing (NIC) on the GCS Supercomputer JUWELS at Jülich Supercomputing Centre (JSC). This research was supported in part through the Maxwell computational resources operated at Deutsches Elektronen-Synchrotron DESY, Hamburg, Germany. We acknowledge the Funding by the Helmholtz Matter and Technologies Accelerator Research and Development Program.

## AUTHOR DECLARATIONS

### Conflict of Interest

The authors have no conflicts to disclose.

### DATA AVAILABILITY

The data that support the findings of this study are available from the corresponding author upon reasonable request.

## APPENDIX: DERIVATION OF THE POTENTIALS IN A PLASMA COLUMN

In the quasi-static approximation, Maxwell's equations can be written as<sup>35</sup>

$$-\nabla_{\perp}^2 \begin{bmatrix} \mathbf{A} \\ \phi \end{bmatrix} = \begin{bmatrix} \mathbf{J} \\ \rho \end{bmatrix}, \quad (\text{A1})$$

with the Lorentz gauge condition being

$$\nabla_{\perp} \cdot \mathbf{A}_{\perp} = \frac{\partial \psi}{\partial \zeta}, \tag{A2}$$

and the wake potential  $\psi = \phi - A_z$ , where  $\phi$  and  $\mathbf{A}$  are the scalar and vector potentials, respectively. Assuming cylindrical symmetry ( $\mathbf{A}_{\perp} = A_r \hat{r}$ ),

$$\frac{1}{r} \frac{\partial}{\partial r} \left( r \frac{\partial}{\partial r} \right) \left[ \frac{\psi}{A_z} \right] = - \left[ \frac{\rho - J_z}{J_z} \right]. \tag{A3}$$

Thus, for a given parameterization of  $\rho$  and  $J_z$ , we can use Eq. (A3) and (A2) to calculate  $\psi$ ,  $A_z$ , and  $A_r$ . Following Ref. 35, we assume: First, the beam expels all electrons within the blowout radius, such that  $\rho$  is solely determined by the ions inside the ion cavity. Note that  $\rho = 0$  for  $R_p < r < R_b$ . Second, the plasma electron sheath density and current can be parameterized by an exponential function and the source term for Eq. (A3) is  $S(\zeta, r) \equiv -(\rho - J_z) \approx -\rho$ , which is consistently observed in PIC simulations. Using the exponential parameterization of the sheath,  $S(\zeta, r)$  in the homogeneous plasma and in the column, with  $R_b < R_p$ , is

$$S(\zeta, r) = \begin{cases} -1, & r < R_b(\zeta), \\ S_0(\zeta) e^{-[r-R_b(\zeta)]/\Delta_p}, & r \geq R_b(\zeta), \end{cases} \tag{A4}$$

with  $S_0(\zeta)$  being the peak and  $\Delta_p$  the thickness of the electron sheath, respectively. In the case of the plasma column with  $R_b \geq R_p$ , the source term is

$$S(\zeta, r) = \begin{cases} -1, & r < R_p < R_b(\zeta), \\ 0, & R_p < r < R_b(\zeta), \\ S_0(\zeta) e^{-[r-R_b(\zeta)]/\Delta_p}, & R_p < R_b(\zeta) < r. \end{cases} \tag{A5}$$

The peak of the source terms  $S_0(\zeta)$  is calculated from Eq. (12) in Ref. 35 and is in the case of a plasma column given by

$$S_0(\zeta) = \begin{cases} \frac{R_b^2(\zeta)}{2\Delta_p [R_b(\zeta) + \Delta_p]}, & R_b(\zeta) < R_p, \\ \frac{R_p^2}{2\Delta_p [R_b(\zeta) + \Delta_p]}, & R_b(\zeta) \geq R_p. \end{cases} \tag{A6}$$

The case  $R_b(\zeta) < R_p$  is equal to  $S_0(\zeta)$  in a homogeneous plasma.

The plasma current density  $J_{z,p}$  is parameterized by

$$J_{z,p}(\zeta, r) = \begin{cases} 0, & r < R_b(\zeta), \\ J_s(\zeta) e^{-[r-R_b(\zeta)]/\Delta_j}, & r \geq R_b(\zeta), \end{cases} \tag{A7}$$

where  $J_s(\zeta)$  is the peak current density and  $\Delta_j$  is the thickness of the sheath current density, respectively.  $J_s(\zeta)$  is calculated by Eq. (16) in Ref. 35 via

$$J_s(\zeta) = \frac{\Lambda(\zeta)/2 - \int_0^{\infty} r dr d^2\Psi/d\zeta^2}{\Delta_j (R_b + \Delta_j)}, \tag{A8}$$

where  $\Lambda(\zeta) = 4I_b/I_A$  is the normalized beam current.

Using the source term, we can calculate  $\psi$  from (A3) by integration and assuming that  $\lim_{r \rightarrow \infty} \psi(r) = 0$ . For the case

$R_p \geq R_b(\zeta)$ , which is equivalent to a homogeneous plasma, we obtain the same result as Ref. 35,

$$\psi(\zeta, r) = \frac{R_b^2 - r^2}{4} + \frac{\Delta_p R_b^2}{2(R_b + \Delta_p)} \left[ 1 + e^{R_b/\Delta_p} E_1 \left( \frac{R_b}{\Delta_p} \right) \right] \tag{A9}$$

for  $r < R_b(\zeta)$  and

$$\psi(\zeta, r) = \frac{\Delta_p R_b^2}{2(R_b + \Delta_p)} e^{-(r-R_b)/\Delta_p} \left[ 1 + e^{r/\Delta_p} E_1 \left( \frac{r}{\Delta_p} \right) \right] \tag{A10}$$

for  $r \geq R_b(\zeta)$ , with  $E_1$  being the exponential integral function. For the case  $R_p < R_b(\zeta)$ , we obtain the new results,

$$\psi(\zeta, r) = \frac{R_p^2 - r^2}{4} + \frac{R_p^2}{2} \log \left( \frac{R_b}{R_p} \right) + \frac{\Delta_p R_p^2}{2(R_b + \Delta_p)} \left[ 1 + e^{R_b/\Delta_p} E_1 \left( \frac{R_b}{\Delta_p} \right) \right]$$

for  $r < R_p < R_b(\zeta)$ ,

$$\psi(\zeta, r) = \frac{\Delta_p R_p^2}{2(R_b + \Delta_p)} \left[ 1 + e^{R_b/\Delta_p} E_1 \left( \frac{R_b}{\Delta_p} \right) \right] + \frac{R_p^2}{2} \left[ \log \left( \frac{R_b}{R_p} \right) - \log \left( \frac{r}{R_p} \right) \right]$$

for  $R_p < r < R_b(\zeta)$ , and

$$\psi(\zeta, r) = \frac{\Delta_p R_p^2}{2(R_b + \Delta_p)} e^{-(r-R_b)/\Delta_p} \left[ 1 + e^{r/\Delta_p} E_1 \left( \frac{r}{\Delta_p} \right) \right] \tag{A11}$$

for  $R_p < R_b(\zeta) < r$ .

For the longitudinal component of the vector potential  $A_z$ , we get the following results both in the plasma column as in the homogeneous plasma. Within the blowout radius  $r < R_b(\zeta)$ ,

$$A_z(\zeta, r) = \frac{\Lambda(\zeta)}{2} \ln r, \tag{A12}$$

and outside of the blowout radius  $r \geq R_b(\zeta)$ ,

$$A_z(\zeta, r) = \frac{\Lambda(\zeta)}{2} \ln r - J_s(\zeta) \Delta_j \left\{ R_b \ln \left( \frac{r}{R_b} \right) + \Delta_j \left[ -1 + \ln \left( \frac{r}{R_b} \right) + e^{-(r-R_b)/\Delta_j} + e^{R_b/\Delta_j} \left( E_1 \left( \frac{r}{\Delta_j} \right) - E_1 \left( \frac{R_b}{\Delta_j} \right) \right) \right] \right\}. \tag{A13}$$

Note that although  $A_z$  has the same form in the column and in the homogeneous case, they still differ, because the peak current  $J_s$  depends on  $\psi$ , which is different in the column and homogeneous case [see Eq. (A8)].

The radial component of the vector potential  $A_r$  in the homogeneous plasma yields within the blowout radius  $r < R_b(\zeta)$ ,

$$A_r(\zeta, r) = \frac{R_b}{4(R_b + \Delta_p)^2} \frac{\partial R_b}{\partial \zeta} (R_b^2 + 2\Delta_p R_b + 2\Delta_p^2) \times r \left[ 1 + e^{R_b/\Delta_p} E_1 \left( \frac{R_b}{\Delta_p} \right) \right], \tag{A14}$$

and outside of the blowout radius  $r \geq R_b(\zeta)$ , we get

$$A_r(\zeta, r) = \frac{R_b}{4(R_b + \Delta_\rho)^2} \frac{\partial R_b}{\partial \zeta} (R_b^2 + 2\Delta_\rho R_b + 2\Delta_\rho^2) \times \frac{1}{r} \left[ R_b^2 + 3\Delta_\rho R_b + 3\Delta_\rho^2 + r^2 e^{R_b/\Delta_\rho} E_1\left(\frac{r}{\Delta_\rho}\right) - 3\Delta_\rho(\Delta_\rho + r) e^{-(r-R_b)/\Delta_\rho} \right]. \quad (\text{A15})$$

Note that there are sign differences between Eqs. (A14) and (A15) and the corresponding Eqs. (21) and (22) in Ref. 35, which do not originate from the choice of co-moving variable. In the column case with  $r, R_p < R_b(\zeta)$ , we obtain the new results

$$A_r(\zeta, r) = \frac{R_b R_p^2}{4(R_b + \Delta_\rho)^2} \frac{\partial R_b}{\partial \zeta} r \left[ 1 + e^{R_b/\Delta_\rho} E_1\left(\frac{R_b}{\Delta_\rho}\right) \right], \quad (\text{A16})$$

and for  $R_p < R_b(\zeta) < r$ ,

$$A_r(\zeta, r) = \frac{R_b R_p^2}{4(R_b + \Delta_\rho)^2} \frac{\partial R_b}{\partial \zeta} \times \frac{1}{r} \left[ R_b^2 + 3\Delta_\rho R_b + 3\Delta_\rho^2 + r^2 e^{R_b/\Delta_\rho} E_1\left(\frac{r}{\Delta_\rho}\right) - 3\Delta_\rho(\Delta_\rho + r) e^{-(r-R_b)/\Delta_\rho} \right]. \quad (\text{A17})$$

## REFERENCES

- <sup>1</sup>E. Esarey, C. B. Schroeder, and W. P. Leemans, "Physics of laser-driven plasma-based electron accelerators," *Rev. Mod. Phys.* **81**, 1229–1285 (2009).
- <sup>2</sup>P. Chen, J. M. Dawson, R. W. Huff, and T. Katsouleas, "Acceleration of electrons by the interaction of a bunched electron beam with a plasma," *Phys. Rev. Lett.* **54**, 693–696 (1985).
- <sup>3</sup>J. B. Rosenzweig, B. Breizman, T. Katsouleas, and J. J. Su, "Acceleration and focusing of electrons in two-dimensional nonlinear plasma wake fields," *Phys. Rev. A* **44**, R6189–R6192 (1991).
- <sup>4</sup>K. V. Lotov, "Blowout regimes of plasma wakefield acceleration," *Phys. Rev. E* **69**, 046405 (2004).
- <sup>5</sup>I. Blumenfeld, C. E. Clayton, F.-J. Decker, M. J. Hogan, C. Huang, R. Ischebeck, R. Iverson, C. Joshi, T. Katsouleas, N. Kirby, W. Lu, K. A. Marsh, W. B. Mori, P. Muggli, E. Oz, R. H. Siemann, D. Walz, and M. Zhou, "Energy doubling of 42 GeV electrons in a metre-scale plasma wakefield accelerator," *Nature* **445**, 741–744 (2007).
- <sup>6</sup>A. J. Gonsalves, K. Nakamura, J. Daniels, C. Benedetti, C. Pieronek, T. C. H. de Raadt, S. Steinke, J. H. Bin, S. S. Bulanov, J. van Tilborg, C. G. R. Geddes, C. B. Schroeder, C. Tóth, E. Esarey, K. Swanson, L. Fan-Chiang, G. Bagdasarov, N. Bobrova, V. Gasilov, G. Korn, P. Sasorov, and W. P. Leemans, "Petawatt laser guiding and electron beam acceleration to 8 GeV in a laser-heated capillary discharge waveguide," *Phys. Rev. Lett.* **122**, 084801 (2019).
- <sup>7</sup>M. Litos, E. Adli, W. An, C. I. Clarke, C. E. Clayton, S. Corde, J. P. Delahaye, R. J. England, A. S. Fisher, J. Frederico, S. Gessner, S. Z. Green, M. J. Hogan, C. Joshi, W. Lu, K. A. Marsh, W. B. Mori, P. Muggli, N. Vafaei-Najafabadi, D. Walz, G. White, Z. Wu, V. Yakimenko, and G. Yocky, "High-efficiency acceleration of an electron beam in a plasma wakefield accelerator," *Nature* **515**, 92–95 (2014).
- <sup>8</sup>C. A. Lindström, J. M. Garland, S. Schröder, L. Boulton, G. Boyle, J. Chappell, R. D'Arcy, P. Gonzalez, A. Knetsch, V. Libov, G. Loisch, A. Martinez de la Ossa, P. Niknejadi, K. Pöder, L. Schaper, B. Schmidt, B. Sheeran, S. Wesch, J. Wood, and J. Osterhoff, "Energy-spread preservation and high efficiency in a plasma-wakefield accelerator," *Phys. Rev. Lett.* **126**, 014801 (2021).
- <sup>9</sup>S. Corde, E. Adli, J. Allen, W. An, C. Clarke, C. Clayton, J. Delahaye, J. Frederico, S. Gessner, S. Green *et al.*, "Multi-gigaelectronvolt acceleration of positrons in a self-loaded plasma wakefield," *Nature* **524**, 442 (2015).
- <sup>10</sup>N. Jain, T. M. Antonsen, Jr., and J. P. Palastro, "Positron acceleration by plasma wakefields driven by a hollow electron beam," *Phys. Rev. Lett.* **115**, 195001 (2015).
- <sup>11</sup>J. Vieira and J. T. Mendonça, "Nonlinear laser driven donut wakefields for positron and electron acceleration," *Phys. Rev. Lett.* **112**, 215001 (2014).
- <sup>12</sup>K. V. Lotov, "Acceleration of positrons by electron beam-driven wakefields in a plasma," *Phys. Plasmas* **14**, 023101 (2007).
- <sup>13</sup>C. B. Schroeder, D. H. Whittum, and J. S. Wurtele, "Multimode analysis of the hollow plasma channel wakefield accelerator," *Phys. Rev. Lett.* **82**, 1177–1180 (1999).
- <sup>14</sup>S. Gessner, E. Adli, J. M. Allen, W. An, C. I. Clarke, C. E. Clayton, S. Corde, J. Delahaye, J. Frederico, S. Z. Green *et al.*, "Demonstration of a positron beam-driven hollow channel plasma wakefield accelerator," *Nat. Commun.* **7**, 11785 (2016).
- <sup>15</sup>C. A. Lindström, E. Adli, J. M. Allen, W. An, C. Beekman, C. I. Clarke, C. E. Clayton, S. Corde, A. Doche, J. Frederico, S. J. Gessner, S. Z. Green, M. J. Hogan, C. Joshi, M. Litos, W. Lu, K. A. Marsh, W. B. Mori, B. D. O'Shea, N. Vafaei-Najafabadi, and V. Yakimenko, "Measurement of transverse wakefields induced by a misaligned positron bunch in a hollow channel plasma accelerator," *Phys. Rev. Lett.* **120**, 124802 (2018).
- <sup>16</sup>S. Zhou, J. Hua, W. An, W. B. Mori, C. Joshi, J. Gao, and W. Lu, "High efficiency uniform wakefield acceleration of a positron beam using stable asymmetric mode in a hollow channel plasma," *Phys. Rev. Lett.* **127**, 174801 (2021).
- <sup>17</sup>T. Silva, L. D. Amorim, M. C. Downer, M. J. Hogan, V. Yakimenko, R. Zgadzaj, and J. Vieira, "Stable positron acceleration in thin, warm, hollow plasma channels," *Phys. Rev. Lett.* **127**, 104801 (2021).
- <sup>18</sup>S. Diederichs, T. J. Mehrling, C. Benedetti, C. B. Schroeder, A. Knetsch, E. Esarey, and J. Osterhoff, "Positron transport and acceleration in beam-driven plasma wakefield accelerators using plasma columns," *Phys. Rev. Accel. Beams* **22**, 081301 (2019).
- <sup>19</sup>S. Diederichs, C. Benedetti, E. Esarey, J. Osterhoff, and C. B. Schroeder, "High-quality positron acceleration in beam-driven plasma accelerators," *Phys. Rev. Accel. Beams* **23**, 121301 (2020).
- <sup>20</sup>E. Adli, C. A. Lindström, J. Allen, C. Clarke, J. Frederico, S. Gessner, S. Green, M. Hogan, M. Litos, B. O'Shea *et al.*, "Long-range attraction of an ultrarelativistic electron beam by a column of neutral plasma," *New J. Phys.* **18**, 103013 (2016).
- <sup>21</sup>P. Muggli, S. Lee, T. Katsouleas, R. Assmann, F.-J. Decker, M. J. Hogan, R. Iverson, P. Raimondi, R. H. Siemann, D. Walz *et al.*, "Refraction of a particle beam," *Nature* **411**, 43–43 (2001).
- <sup>22</sup>P. Muggli, S. Lee, T. Katsouleas, R. Assmann, F. J. Decker, M. J. Hogan, R. Iverson, P. Raimondi, R. H. Siemann, D. Walz, B. Blue, C. E. Clayton, E. Dodd, R. A. Fonseca, R. Hemker, C. Joshi, K. A. Marsh, W. B. Mori, and S. Wang, "Collective refraction of a beam of electrons at a plasma-gas interface," *Phys. Rev. ST Accel. Beams* **4**, 091301 (2001).
- <sup>23</sup>K. Lotov, "Force exerted on particle bunch propagating near plasma-vacuum boundary," *Plasma Phys. Controlled Fusion* **62**, 085002 (2020).
- <sup>24</sup>W. An, M. Zhou, N. Vafaei-Najafabadi, K. A. Marsh, C. E. Clayton, C. Joshi, W. B. Mori, W. Lu, E. Adli, S. Corde, M. Litos, S. Li, S. Gessner, J. Frederico, M. J. Hogan, D. Walz, J. England, J. P. Delahaye, and P. Muggli, "Strategies for mitigating the ionization-induced beam head erosion problem in an electron-beam-driven plasma wakefield accelerator," *Phys. Rev. ST Accel. Beams* **16**, 101301 (2013).
- <sup>25</sup>V. Yakimenko, L. Alsberg, E. Bong, G. Bouchard, C. Clarke, C. Emma, S. Green, C. Hast, M. J. Hogan, J. Seabury, N. Lipkowitz, B. O'Shea, D. Storey, G. White, and G. Yocky, "FACET-II facility for advanced accelerator experimental tests," *Phys. Rev. Accel. Beams* **22**, 101301 (2019).
- <sup>26</sup>D. H. Whittum, W. M. Sharp, S. S. Yu, M. Lampe, and G. Joyce, "Electron-hose instability in the ion-focused regime," *Phys. Rev. Lett.* **67**, 991–994 (1991).
- <sup>27</sup>C. Huang, W. Lu, M. Zhou, C. E. Clayton, C. Joshi, W. B. Mori, P. Muggli, S. Deng, E. Oz, T. Katsouleas, M. J. Hogan, I. Blumenfeld, F. J. Decker,

- R. Ischebeck, R. H. Iverson, N. A. Kirby, and D. Walz, "Hosing instability in the blow-out regime for plasma-wakefield acceleration," *Phys. Rev. Lett.* **99**, 255001 (2007).
- <sup>28</sup>V. E. Balakin, A. V. Novokhatsky, and V. P. Smirnov, "VLEPP: Transverse beam dynamics," in *Proceedings of the 12th International Conference on High-Energy Accelerators, HEACC 1983: Fermilab, Batavia, August 11–16, 1983* (1983), Vol. C830811, pp. 119–120.
- <sup>29</sup>T. J. Mehrling, R. A. Fonseca, A. Martinez de la Ossa, and J. Vieira, "Mitigation of the hose instability in plasma-wakefield accelerators," *Phys. Rev. Lett.* **118**, 174801 (2017).
- <sup>30</sup>W. An, W. Lu, C. Huang, X. Xu, M. J. Hogan, C. Joshi, and W. B. Mori, "Ion motion induced emittance growth of matched electron beams in plasma wakefields," *Phys. Rev. Lett.* **118**, 244801 (2017).
- <sup>31</sup>T. J. Mehrling, C. Benedetti, C. B. Schroeder, E. Esarey, and W. P. Leemans, "Suppression of beam hosing in plasma accelerators with ion motion," *Phys. Rev. Lett.* **121**, 264802 (2018).
- <sup>32</sup>A. Martinez de la Ossa, T. J. Mehrling, and J. Osterhoff, "Intrinsic stabilization of the drive beam in plasma-wakefield accelerators," *Phys. Rev. Lett.* **121**, 064803 (2018).
- <sup>33</sup>T. J. Mehrling, C. Benedetti, C. B. Schroeder, A. Martinez de la Ossa, J. Osterhoff, E. Esarey, and W. P. Leemans, "Accurate modeling of the hose instability in plasma wakefield accelerators," *Phys. Plasmas* **25**, 056703 (2018).
- <sup>34</sup>W. Lu, C. Huang, M. Zhou, W. B. Mori, and T. Katsouleas, "Nonlinear theory for relativistic plasma wakefields in the blowout regime," *Phys. Rev. Lett.* **96**, 165002 (2006).
- <sup>35</sup>S. A. Yi, V. Khudik, C. Siemon, and G. Shvets, "Analytic model of electromagnetic fields around a plasma bubble in the blow-out regime," *Phys. Plasmas* **20**, 013108 (2013).
- <sup>36</sup>A. A. Golovanov, I. Y. Kostyukov, J. Thomas, and A. Pukhov, "Analytic model for electromagnetic fields in the bubble regime of plasma wakefield in non-uniform plasmas," *Phys. Plasmas* **24**, 103104 (2017).
- <sup>37</sup>T. N. Dalichaouch, X. L. Xu, A. Tableman, F. Li, F. S. Tsung, and W. B. Mori, "A multi-sheath model for highly nonlinear plasma wakefields," *Phys. Plasmas* **28**, 063103 (2021).
- <sup>38</sup>S. Diederichs, C. Benedetti, A. Huebl, R. Lehe, A. Myers, A. Sinn, J.-L. Vay, W. Zhang, and M. Thévenet, "HiPACE++: a portable, 3D quasi-static particle-in-cell code," *Comput. Phys.* (in press); [arXiv:2109.10277](https://arxiv.org/abs/2109.10277).
- <sup>39</sup>J. B. Rosenzweig, A. M. Cook, A. Scott, M. C. Thompson, and R. B. Yoder, "Effects of ion motion in intense beam-driven plasma wakefield accelerators," *Phys. Rev. Lett.* **95**, 195002 (2005).
- <sup>40</sup>C. Benedetti, C. B. Schroeder, E. Esarey, and W. P. Leemans, "Emittance preservation in plasma-based accelerators with ion motion," *Phys. Rev. Accel. Beams* **20**, 111301 (2017).
- <sup>41</sup>C. Benedetti, T. J. Mehrling, C. B. Schroeder, C. G. R. Geddes, and E. Esarey, "Adiabatic matching of particle bunches in a plasma-based accelerator in the presence of ion motion," *Phys. Plasmas* **28**, 053102 (2021).
- <sup>42</sup>R. Lehe, C. B. Schroeder, J.-L. Vay, E. Esarey, and W. P. Leemans, "Saturation of the hosing instability in quasilinear plasma accelerators," *Phys. Rev. Lett.* **119**, 244801 (2017).
- <sup>43</sup>S. Diederichs, C. Benedetti, M. Thévenet, E. Esarey, and C. B. Schroeder, "Self-stabilizing positron acceleration in a plasma column," (submitted).